PAPER

Check for updates

A sustainable approach for the adsorption of methylene blue from an aqueous background: an adsorbent based on DES/CGS modified GO@ZrO₂†

Vishwajit Chavda, [a] Brijesh Patel,[a] Sneha Singh,[a] Darshna Hirpara, [a] V. Devi Rajeswari[b] and Sanjeev Kumar [*a]

Gemini surfactants (GSs) and deep eutectic solvents (DESs) belong to two important classes of industrially important materials which can be used to modify the performances of other entities where they are used for functionalization. A graphene oxide-zirconium oxide (GO@ZrO₂) nanocomposite has been synthesised and modified by using a cationic gemini surfactant (CGS, butanediyl-1,4, bis(*N*,*N*-hexadecyl ammonium) dibromide (16-4-16)) or by using a well-known DES (reline, choline chloride : urea, molar ratio 1 : 2). The adsorbent materials were characterized by various physicochemical techniques (FTIR, XRD, TEM, SEM-EDX, and TGA). Methylene blue (MB), a well-known industrially important colouring material, has been used as a model adsorbate to investigate its adsorption/removal from aqueous solution by using the above-modified nanocomposites (NCs, CGS-GO@ZrO₂ and DES-GO@ZrO₂). The adsorption process follows the Langmuir model ($R^2 \approx 0.995$) together with *pseudo*-second order rate kinetics. Adsorption variables were optimised in the light of [NC], [MB], pH, and contact time. DES-GO@ZrO₂ has been found to be a better candidate for the fast removal of MB (~100% at 20 mg L^{-1}, 5 m with 2 mg ml^{-1} DES-GO@ZrO₂) when compared with other similarly modified materials. To economize the method, desorption of adsorbed MB (performed by using ethanol) is necessary. It has been found that the DES-GO@ZrO₂ performs efficiently even after 5 adsorption–desorption series. The findings of the present study can have potential applications in developing an economic strategy for the purification of industrial dye effluents with a concomitant redressal of aquatic pollution.

Sustainability spotlight

Industrial effluents containing colour and colouring materials pose a significant threat to the aquatic ecosystem, with dyes from textile industries being a major contributor. To save running water sources from contamination, it is desirable to search for effective strategies for removing dyes from industrial wastewater. In response to this challenge, a sustainable and economically viable answer emerges in the form of modified graphene-based composites. This innovative idea not only offers valuable insights but also presents a practical solution for mitigating the harmful effects of dye effluents. By adopting the methodology presented here, one can actively conserve the already present limited potable water resources on mother earth.

1 Introduction

The last 4–5 decades witnessed a sharp increase in the fundamental progress and prospects of various kinds of materials such as nanomaterials, electronic materials, solvent materials, associated materials, membrane materials, and porous materials among others.[1–11] Among these materials, carbon allotropes attract special attention due to their novel properties and potential application in various fields of life.[12–16] Graphene is the most sought-after carbon allotrope, both in its pure form and when incorporated into composite materials or utilized in its derived forms, in various areas of scientific and engineering research.[4,17–20] Graphene is a uni-layer bi-dimensional surface of carbon atoms chemically bonded in the sp² configuration with a hexagonal pattern (benzene ring).[17,18] However, graphene oxide (GO) is preferred over graphene due to the presence of functional groups, though graphene has exceptional mechanical, electrical, and thermal properties.[21]

GO spontaneously distributes in an aqueous medium facilitating polluted water treatment.[22,23] Furthermore, GO shows high electronic mobility imparted from oxygenated moieties at the basal plane and edges.[24] However, high surface energy results in agglomeration and lower dispersibility as well as

ªDepartment of Applied Chemistry, Faculty of Technology & Engineering, The Maharaja Sayajirao University of Baroda, Vadodara – 390 002, Gujarat, India. E-mail: drksanjeev@gmail.com; sanjeevkumar-appchem@msubaroda.ac.in

ᵇDepartment of Biomedical Sciences, School of Biosciences and Technology, VIT University, Vellore – 14, Tamil Nadu, India

† Electronic supplementary information (ESI) available. See DOI: https://doi.org/10.1039/d3su00236e

Table 1 Fitted kinetic data in different models for DES-GO@ZrO$_2$ and CGS-GO@ZrO$_2$

Adsorbent (mg L^{-1})	Pseudo-first order				Pseudo-second order			Intra-particle diffusion		
	Q_e (exp) (mg g^{-1})	Q_e (cal) (mg g^{-1})	k_1 (min^{-1})	R^2	Q_e (cal) (mg g^{-1})	k_2 (g mg^{-1} min^{-1})	R^2	k_i	C_i	R^2
DES-GO@ZrO$_2$										
20	9.88	9.92	0.087	0.885	9.94	1.065	0.999	2.412	2.69	0.620
40	19.93	18.76	0.035	0.239	20.99	0.019	0.993	2.272	5.88	0.765
60	29.84	22.55	0.596	0.113	31.66	0.033	0.967	2.197	5.99	0.921
80	39.89	23.56	0.113	0.387	41.52	0.004	0.979	2.687	11.21	0.857
100	47.85	25.36	0.067	0.209	54.43	0.001	0.896	3.584	3.02	0.968
CGS-GO@ZrO$_2$										
10	0.86	0.745	0.011	0.909	0.98	0.668	0.988	0.233	0.10	0.603
50	3.28	3.184	0.063	0.864	33.70	0.001	0.913	0.897	0.47	0.529
100	9.33	10.14	0.011	0.655	10.81	0.154	0.999	1.395	3.55	0.861
1000	72.13	58.35	0.034	0.716	72.83	0.002	0.998	3.663	28.71	0.825

applicability.[25] Such inefficiencies of GO can be resolved by its fusion with some metallic oxides by anchoring a nano-composite (NC) into its skeleton which may address and modify the existing problem and properties, respectively.[26–30] Nano-composites are known as multicomponent materials with different phase nano-domains.[31] Compared with GO, the above nanocomposites show specific architectural morphology and photochemical characteristics and exhibit good performance towards water treatment technologies.[32] Among various metal oxides used for composite formation, zirconia (ZrO$_2$) has attracted researchers due to its passive nature and lower reductive potential together with lower processing cost.[33] It has been reported that GO-based metal composites are preferably used for the removal of cationic pollutants while very rarely used for the anionic moieties.[34] Currently, NCs are modified with a variety of compounds/mixtures (synthetic and natural polymers and surfactants) owing to their field of application.[34–41]

In the above context, surfactants are preferred as modification agents due to their simple synthesis process, improved crystallinity/thermal stability, prevention of agglomeration, and the increased surface area and controlled porosity of the resulting modified material.[42–47] Cationic surfactants have found use as preferred modifiers in comparison to other charge type ones.[45,48–50] Recently, a cationic gemini surfactant (CGS) was reported as a modification material.[51–56] CGSs are known for showing improved structural and surface/solution properties over conventional cationic surfactants.[57–65] These research studies show that CGSs can be used to modify metal oxide or GO to facilitate the adsorption/degradation phenomenon. The utilization of CGS modified nanocomposites, based on metal oxide and GO, has been reported only a few times.[40,66]

A new solvent material denoted as deep eutectic solvent (DES), has been introduced as a substitute for ionic liquids with added superior properties.[67–70] DES is now gaining momentum as a potential modifier in nanomaterial synthesis, processing, and functionalization of NCs.[71–78] These materials are safe, accessible, green, and environmentally friendly, and show increased affinity towards the materials of interest.[76,79] On the

basis of the above survey, it seems of genuine interest to compare the adsorption efficiencies of CGS and DES modified NCs.

Saving pure water bodies, for the next generation, on the earth, is the biggest challenge to the research community.[80–84] World bank data show that textile waste (*e.g.*, colour or colour-causing material) contributes ~20% of the total industrial water pollution.[85] Thus, the colour/colouring compound eradication from the effluent is the first and foremost challenge faced by industries worldwide. This boosts the search for an optimised treatment method in order to diminish colouring pollutants from the effluent, before mixing in the regular potable water streams. NCs have been shown to be used as a potential material to solve the above mentioned problem using various modifications.[26,86–90] Owing to the economic and synthetic characteristics of ZrO$_2$ and DES, respectively, both are chosen for NC synthesis with GO and for further functionalization (DES-GO@ZrO$_2$). Moreover, another similar composite has been synthesised and modified with CGS using a method reported elsewhere.[40] Methylene blue (MB) is used as a model dye for the adsorption/kinetic study. Butanediyl-1,4, bis(*N*,*N*-hexadecyl ammonium) dibromide (16-4-16) and reline are used as the CGS and DES, respectively, for the current study. Reline is a well-known DES that can be obtained by mixing (1 : 2, molar ratio) choline chloride (ChCl), as a hydrogen bond acceptor (HBA), and urea, as a hydrogen bond donor (HBD).[91] Modified NCs were characterized by different methods such as Fourier transform infrared spectroscopy (FT-IR), X-ray diffraction (XRD), transmission electron microscopy (TEM), scanning electron microscopy-energy dispersive X-ray analysis (SEM-EDX), and thermogravimetric analysis (TGA). Various experimental conditions are optimised (NC doses, contact time, pH, initial adsorbate content, *etc.*) in order to realize the maximum removal of dyes from the aqueous medium. Probably, such type of comparative work on CGS/DES modified NCs has been performed for the first time. The strategies reported here may find application in reducing water pollution and cleaning the environment in general.

2 Materials and methods

2.1 Chemicals

GO, CGS, and DES (reline) are synthesised and characterized using the same procedures as reported previously.[40,58,92] Zirconium acetate [$Zr(CH_3COO)_2$] (99%) has been purchased from Loba Chemie, India, and used as received. ChCl (99%) has been obtained from TCI (India) and was used after vacuum drying (40 $\pm$ 0.5 °C). Urea has been obtained (99%) from Sigma Aldrich and used with no further purification. Methylene blue (MB), of microscopic grade (98%), was obtained from Loba Chemie, India. Distilled water of specific conductance ~1 μS cm^{-1} was used throughout. All the other reagents and chemicals used are of AR grade. The chemical structures of 16-4-16 (CGS), reline (DES), and MB are given in Scheme 1.

2.2 Preparation of GO@ZrO_2 NC

GO was synthesised by using a well-established modified Hummers method.[93,94] Synthesis of GO@ZrO$_2$ involves the following steps: GO has been dispersed in an aqueous solution (1 g in 100 ml) through sonication for 30 m. The resulting dispersion was mixed with aqueous zirconium acetate (1 g in 100 ml) and stirring was performed for 30 m. Subsequently, the mixture was again sonicated for 1 h and 20 ml 1 M NaOH was added gradually. The resulting mixture was heated to 100 $\pm$ 0.1 °C and stirred for another 2 h. A colour change from greenish yellow to black indicates the formation of the dispersed aqueous GO@ZrO$_2$ NC. The latter was filtered and the solid mass was washed thrice with distilled water and then ethanol (50 ml each). The material, GO@ZrO$_2$ NC, was dried in a vacuum oven (100 $\pm$ 0.5 °C) for 12 h which resulted in a black shiny powder.

2.3 Modification of GO@ZrO_2 using CGS

The above synthesised GO@ZrO$_2$ was modified with CGS using the following procedure. GO@ZrO$_2$ (3 g/100 ml) was stirred in aqueous CGS solution (0.1 g/100 ml). The resulting mixture was sonicated for 5 m and then gently stirred for another 2 h at room temperature. The resulting dispersion was subsequently centrifuged (3000 rpm for 10 m) and washed thrice with distilled water (50 ml each time). This gives a CGS-modified NC (CGS-GO@ZrO$_2$) after drying in a vacuum oven at 65 $\pm$ 0.5 °C for 12 h.

2.4 Modification of GO@ZrO_2 using reline as the DES

1 g of GO@ZrO$_2$ was sonicated with 10 ml of DES (reline) for 30 m to get a homogenous dispersion. This dispersion has been transferred into a round bottom flask and then stirred at 80 $\pm$ 0.1 °C for 2 h. The mixture was filtered and washed thrice with distilled water followed by ethanol (50 ml of each). This DES-modified NC (DES-GO@ZrO$_2$) was dried in a vacuum oven for 24 h at 80 $\pm$ 0.5 °C.

2.5 Instrumentation for characterisation of the synthesised/modified NCs

X-ray diffraction (XRD) spectra of GO@ZrO$_2$, CGS-GO@ZrO$_2$, and DES-GO@ZrO$_2$ powder NCs have been recorded on an X-ray

Methylene blue

Graphene Oxide

Reline

16-4-16
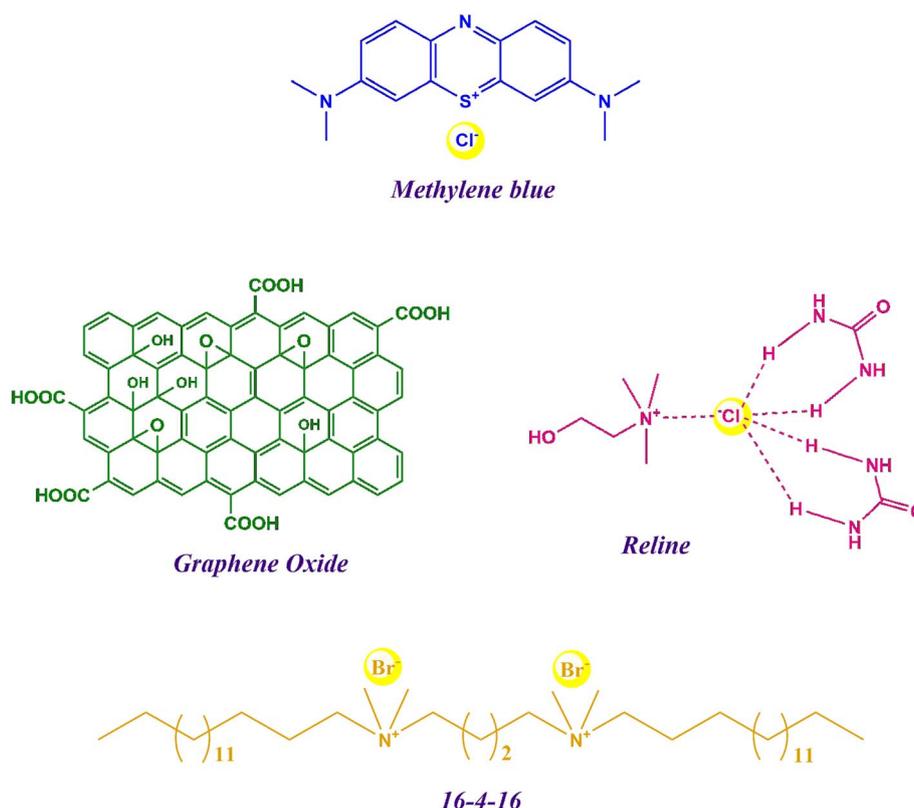
Scheme 1 Chemical structures of various materials used in the study.

diffractometer (SmartLab, Rigaku Corporation, Japan, operating at 40 kV) equipped with a Cu laser source at a scanning rate of 2° m⁻¹ within a range of 5° to 80°. FT-IR spectra of various NCs were recorded in the range of 400–4000 cm⁻¹ on an FTIR-8400S, Shimadzu, Japan. TEM has been used to obtain morphological information by using a TEM-1400 PLUS, Jeol India Pvt. Ltd., India. For the TEM grid preparation, 1 mg of each NC sample has been sonicated in 20 ml of pure ethanol for 30 m using a tip sonicator, followed by placing two drops of the resulting suspension on a carbon-coated copper grid (200 mesh). The prepared TEM grid was air-dried for 30 m at room temperature before the TEM imaging experiment. The surface morphologies and elemental composition of the NC samples were studied using SEM (Hitachi SU70 SEM, Japan) at 15 kV coupled with EDX (EDX-8100, Shimadzu, Japan). Thermal stabilities of the synthesised/modified NCs were estimated using the TGA technique (TGA 50, Shimadzu, Japan) by collecting thermograms in the temperature range between 25 and 700 °C (heating rate of 10 °C m⁻¹) under a nitrogen atmosphere.

2.6 Dye adsorption study

Adsorption data are acquired by adopting a batch experiment approach (in triplicate). The concentration of MB has been quantified using an external calibration method (λ_{max} = 663 nm). A good correlation line (not shown) has been obtained (R^2 ∼ 0.999) and is thus used for quantifying MB adsorption. The solution of dye (20 ml) of an appropriate concentration (10–1000 mg L⁻¹) was mixed with different composite dosages (1–15 mg ml⁻¹) in quick-fit glass bottles. The mixture was kept under ambient conditions for different periods of time

depending upon the nature of the study (adsorption or kinetics). The equilibrated (after the stipulated interval) mixture was centrifuged before UV-vis investigation (UV-1800, Shimadzu, Japan). The composite adsorption capacity (Q) has been computed using the following expression,

$$Q = \frac{(C_i - C_t)}{C_i} \times \frac{V}{w} \tag{1}$$

where C_i and C_t are the initial and at time t concentrations of MB, respectively, V is the volume of MB solution and w is the weight of the modified composite (adsorbent). Furthermore, the percentage of dye removal (P) has been estimated by using the following mathematical expression,

$$P = \frac{(C_i - C_t)}{C_i} \times 100 \tag{2}$$

2.7 Determination of pH at the point of zero charge (pH$_{pzc}$)

The salt addition method[95] was used to determine the pH$_{pzc}$ of DES-GO@ZrO$_2$ and CGS-GO@ZrO$_2$ using 0.1 M KNO$_3$ solution at 30 ± 0.1 °C. The total volume of the solution was adjusted exactly to 20 ml in a conical flask by adding 0.1 M KNO$_3$. The initial pH (pH$_{initial}$) of the solutions was adjusted between 2.0 and 12.0 by adding 0.1 M HCl and 0.1 M NaOH solutions, respectively. The solutions of different pH$_{initial}$ values were then mixed with 50 mg NC, and the suspension was allowed to stand for 24 h. The final pH (pH$_{final}$) of the supernatant liquid was noted for each solution. The difference between the pH$_{initial}$ and pH$_{final}$ (ΔpH = pH$_{initial}$ − pH$_{final}$) was then plotted against

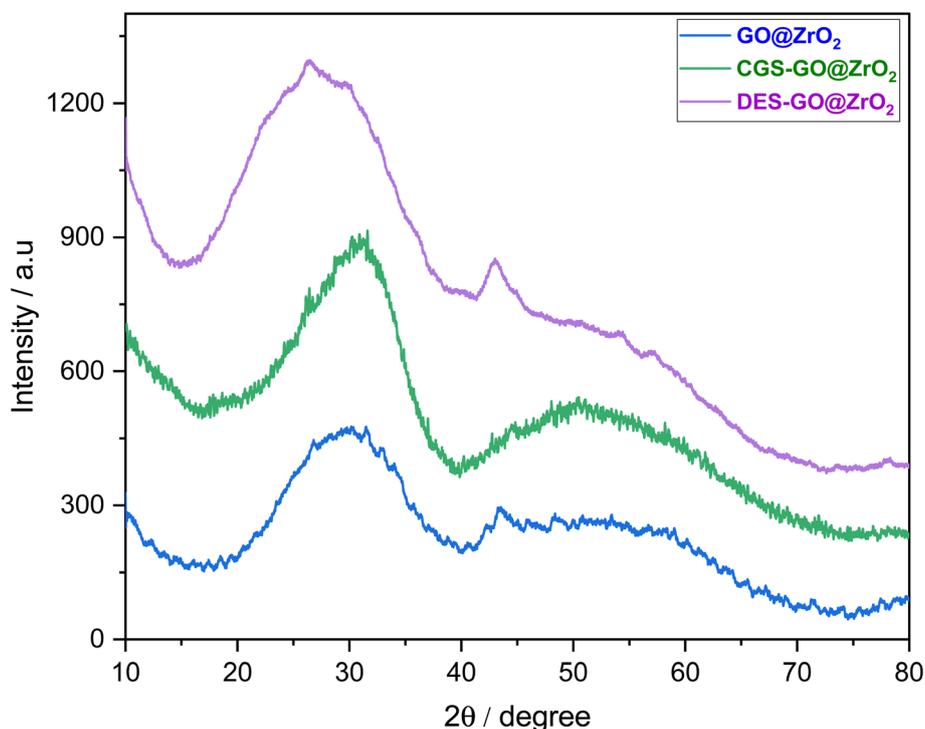**Fig. 1** XRD spectra of the modified nanocomposite(s) and its precursor.

$pH_{initial}$. The point of intersection of the resulting curve with the abscissa, at which $\Delta pH = 0$, gives the pH_{pzc}.

2.8 Dye re-adsorption study

The adsorbed MB has been separated from the adsorbent by washing (3 times) with 50 ml ethanol each time. With each washing, the adsorbent was filtered. The washed adsorbent was then dried in a vacuum oven at 80 °C for 12 h. The so-obtained recharged DES-GO@ZrO$_2$ has been used (up to the 5th cycle) for the re-adsorption of MB. R_e-adsorption efficiency (R_e) has been computed by using the below-mentioned expression,

$$R_e = \frac{Q_r}{Q_f} \times 100 \tag{3}$$

where Q_r and Q_f are adsorption capacities with recharged and fresh DES-GO@ZrO$_2$.

3 Results and discussion

3.1 Characterisation of the synthesised/modified NCs

XRD spectra of all the NCs are shown in Fig. 1. The broadness of NC spectra indicates poor crystallinity (amorphousness) of all NCs. When XRD data were compared with those of pure GO and pure ZrO$_2$ (Fig. S1, ESI†), the composite material has been found to be more amorphous than the individual components. Similar types of signals were observed for the controlled deposition of ZrO$_2$ on graphene nanosheets in earlier studies.[96,97] Fig. 1 also shows that amorphousness more or less remained similar even after modification with CGS or DES. In an earlier study, it has been shown that a surfactant modified NC-material shows more amorphousness than pure GO and corroborates the present data.[98]

FT-IR spectra of GO@ZrO$_2$, CGS-GO@ZrO$_2$, and DES-GO@ZrO$_2$ are compiled in Fig. 2. In the case of CGS-GO@ZrO$_2$, the appearance of peaks at around 2923 and 2847 cm^{-1} indicates the existence of C–H stretching vibration bands and confirms the presence of the CGS alkyl group and hence the modification of GO@ZrO$_2$ by CGS. Similarly, in the case of DES-GO@ZrO$_2$, peaks appear at 3019 and 3261 cm^{-1} which are expected to be from the vibrations of H-bonds in O–H and/or N–H, as reported earlier.[99] Furthermore, Zr–O bands appeared at 635 cm^{-1} and 762 cm^{-1}. The absorption band which appeared at 2900 cm^{-1} indicates a small alkyl chain of the choline part of reline present at the surface of DES-GO@ZrO$_2$.

TEM images of pure GO@ZrO$_2$ and modified NCs are shown in Fig. 3. Modified composite images (Fig. 3b and c) show wrinkles and folding on the outer part of the original composite. The sheets are comparatively well separated for DES-GO@ZrO$_2$ than for CGS-GO@ZrO$_2$ (for the same magnification).

SEM-EDX data are given in Fig. 4 to further ensure the modification of GO@ZrO$_2$. The elemental analysis data are summarized in the ESI (Table S1†). The presence of nitrogen and chlorine atoms in the modified composites shows the functionalization of GO@ZrO$_2$ with CGS or DES (as the case may be). The data are indicative of the successful functionalization of the GO@ZrO$_2$ NC.
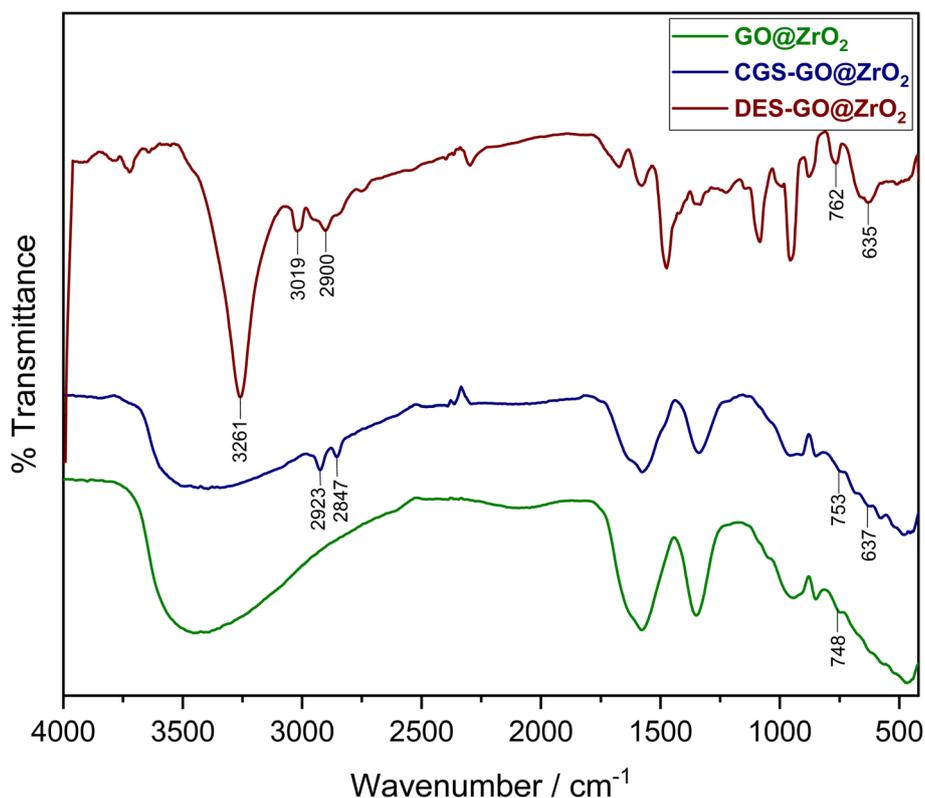

Fig. 2 FT-IR spectra of GO@ZrO$_2$ and its modified forms with CGS and DES nanocomposites.
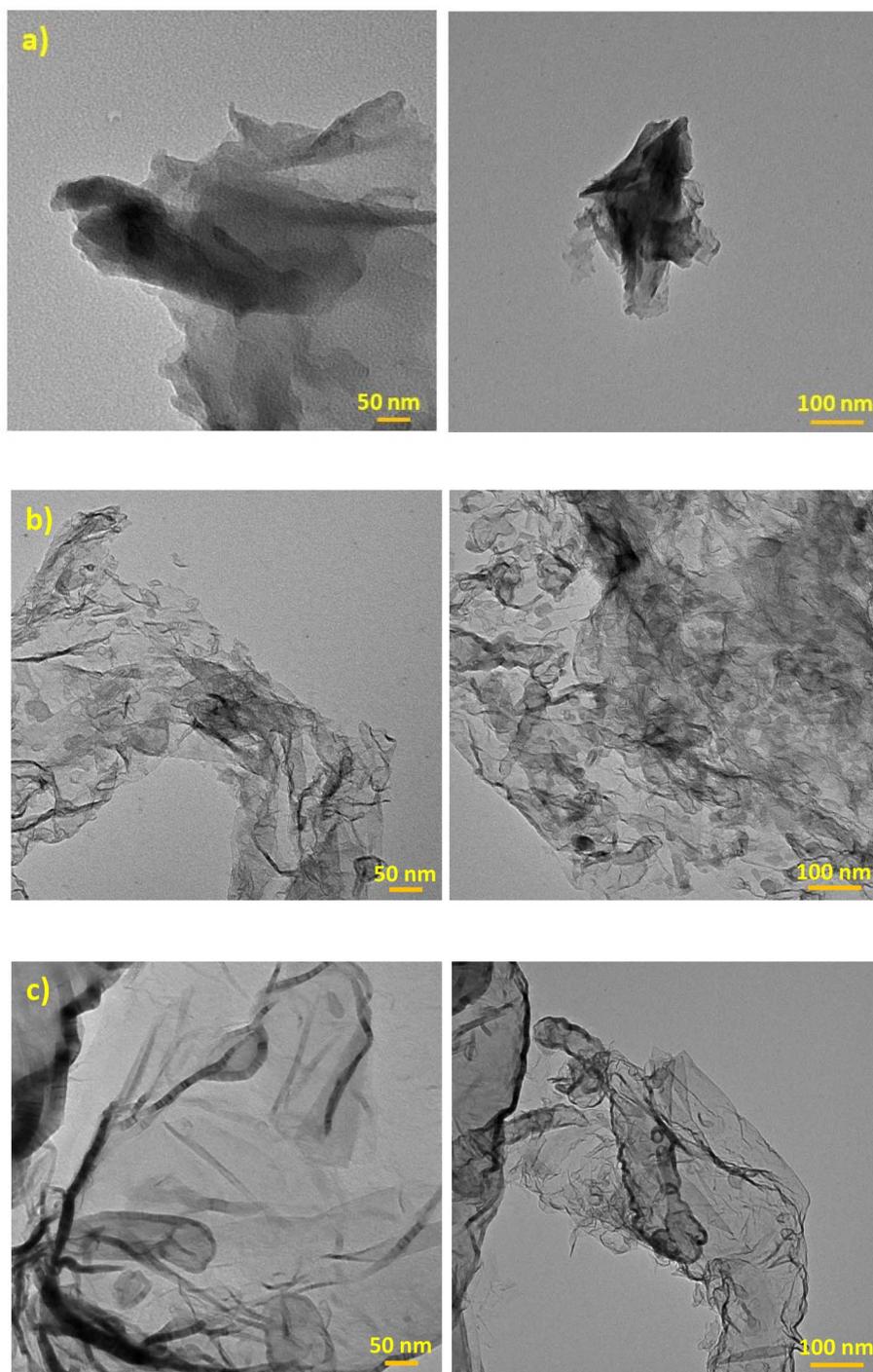
© 2023 The Author(s). Published by the Royal Society of Chemistry

Fig. 3 TEM images of (a) GO@ZrO$_2$, (b) CGS-GO@ZrO$_2$, and (c) DES-GO@ZrO$_2$.

TGA thermograms and derivative thermograms for pure and functionalized nanocomposites are provided in Fig. 5a and b, respectively. Thermal stability of GO@ZrO$_2$ increases with both CGS/DES modified NCs. This additional thermal stability in the presence of both DES and CGS indicates that the decomposition of labile surface oxygens is restricted. This surface stability can be further utilized for higher temperature adsorption if needed.

3.2 Influence of [MB]

Removal of MB (by an adsorption process) from aqueous dye solution (without agitation) was studied in the presence of a fixed dose of the composite (GO@ZrO$_2$ (2 mg ml^{-1}), CGS-GO@ZrO$_2$ (10 mg ml^{-1}) or DES-GO@ZrO$_2$ (2 mg ml^{-1})). The percentage of MB removal (P) in all the cases (after 60 m, followed by centrifugation) has been plotted against different fixed [MB] (20–100 mg L^{-1}), and data are depicted in Fig. 6. The
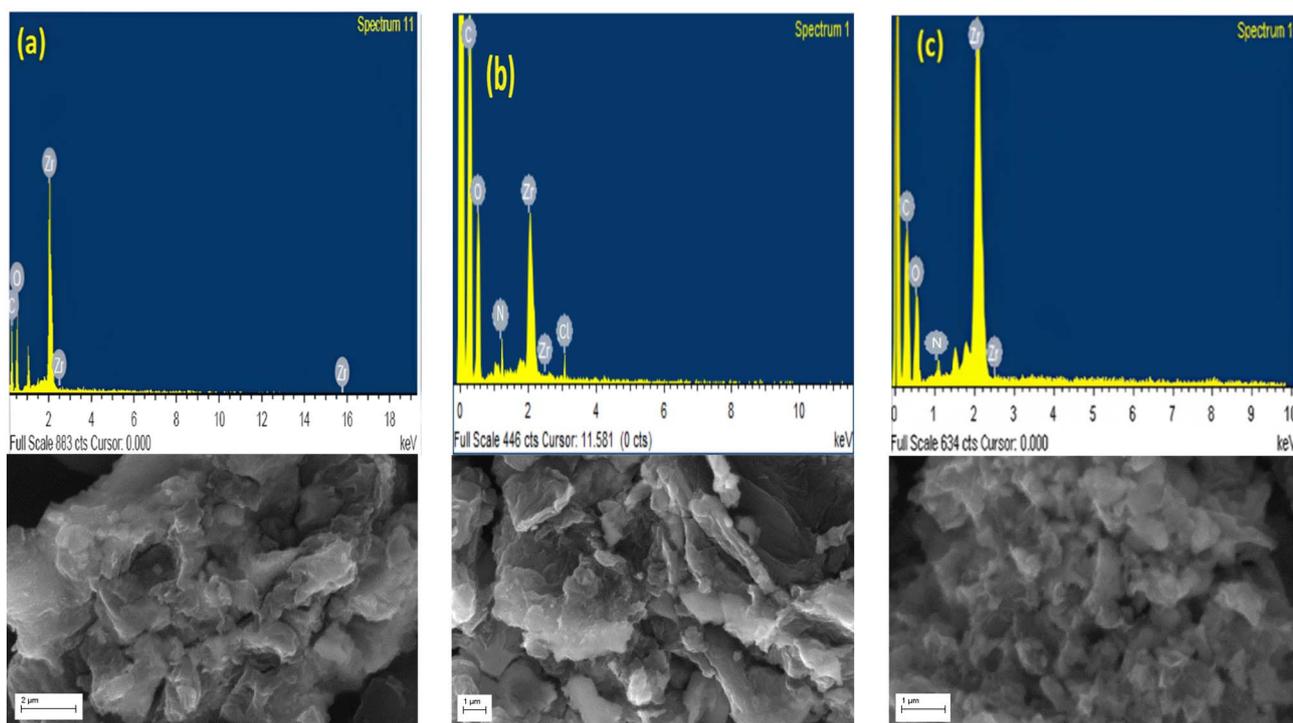
Fig. 4 SEM-EDX images of (a) GO@ZrO$_2$, (b) DES-GO@ZrO$_2$ and (c) CGS-GO@ZrO$_2$.

perusal of data (Fig. 6) suggests that modification improves the P value compared to that observed with GO@ZrO$_2$. It may be mentioned that DES-GO@ZrO$_2$, even having 5 times lower quantity, competes well for the initial lower [MB] ($\sim$40 mg L^{-1}). However, at further higher [MB], the P values show distinct differences for the above two modified NCs. Preliminary adsorption data show the competitiveness of DES modified NC with the CGS one. In this experiment, the best performances of MB adsorption were found at 20 mg L^{-1} and 50 mg L^{-1} for DES-GO@ZrO$_2$ and CGS-GO@ZrO$_2$, respectively. Therefore, these concentrations were taken to optimise the composite dosages.

3.3 Influence of the composite load

The above fixed MB concentrations were used to study the influence of the composite load on the absorbability of MB from an aqueous solution. The NC load has been varied to determine the appropriate content of the adsorbent in the removal of MB (after 60 m) together with Q. Data for DES-GO@ZrO$_2$ and CGS-GO@ZrO$_2$ are shown in Fig. 7. A perusal of the data indicates that a near complete MB adsorption has been observed at/above 2 mg ml^{-1} with the former NC while similar MB adsorption was observed at/above 10 mg ml^{-1} for the latter NC (CGS-GO@ZrO$_2$). Therefore, 2 mg ml^{-1} composite load and 20 mg L^{-1} MB concentration have been fixed for DES-GO@ZrO$_2$ while 10 mg ml^{-1} composite load and 50 mg L^{-1} MB concentration were fixed for CGS-GO@ZrO$_2$ to study the influence of pH.

3.4 Influence of pH

pH variation has been accomplished by varying the concentration of NaOH/HCl depending upon the pH range (basic or acidic). With an increase in pH, MB molecules will exist in both charged and uncharged forms. The variation of P vs. pH for the above-mentioned systems (Section 3.2, after 60 m) is shown in Fig. 8. P has been found to be lower in a higher acidic range and increases with an increase in pH and shows distinctly higher MB adsorption (or P) at pH 10 for DES-GO@ZrO$_2$. This may be interpreted in terms of the conversion of the cationic MB form into the neutral MB form. The latter form may be driven towards the NC surface due to the hydrophobic attraction of the dye towards modified NC surfaces. Fig. 9 shows the variation of ΔpH vs. pH$_{initial}$ and resulted in pH$_{pzc}$ zero between pH 7 to 8. Beyond this pH range the NC surface will be negatively charged and start attracting the cationic form of the dye and be responsible for a sudden increase in the P value from pH 8–10. This could also be understood in light of the fact that the pK_a value of MB is 3.8.[100] The increase in the P value with pH finds support in an earlier study in which MB adsorption has been conducted on a GO-based composite.[26] However, the amount of MB adsorbed from pH 4–8 for CGS-GO@ZrO$_2$ is nearly constant. The former form will interact electrostatically with the CGS-GO@ZrO$_2$ surface while the latter one will interact hydrophobically. The overall adsorption might be the result of the above two interactions and works oppositely for CGS-GO@ZrO$_2$ and is responsible for a level-off in the P value. This is indeed observed in Fig. 8.

3.5 Influence of contact time: adsorption kinetics

In order to understand the kinetics of the adsorption process, influences of contact time and [MB] have been seen at a fixed concentration of composite (2 or 10 mg ml^{-1}) and pH ($=$10). Q
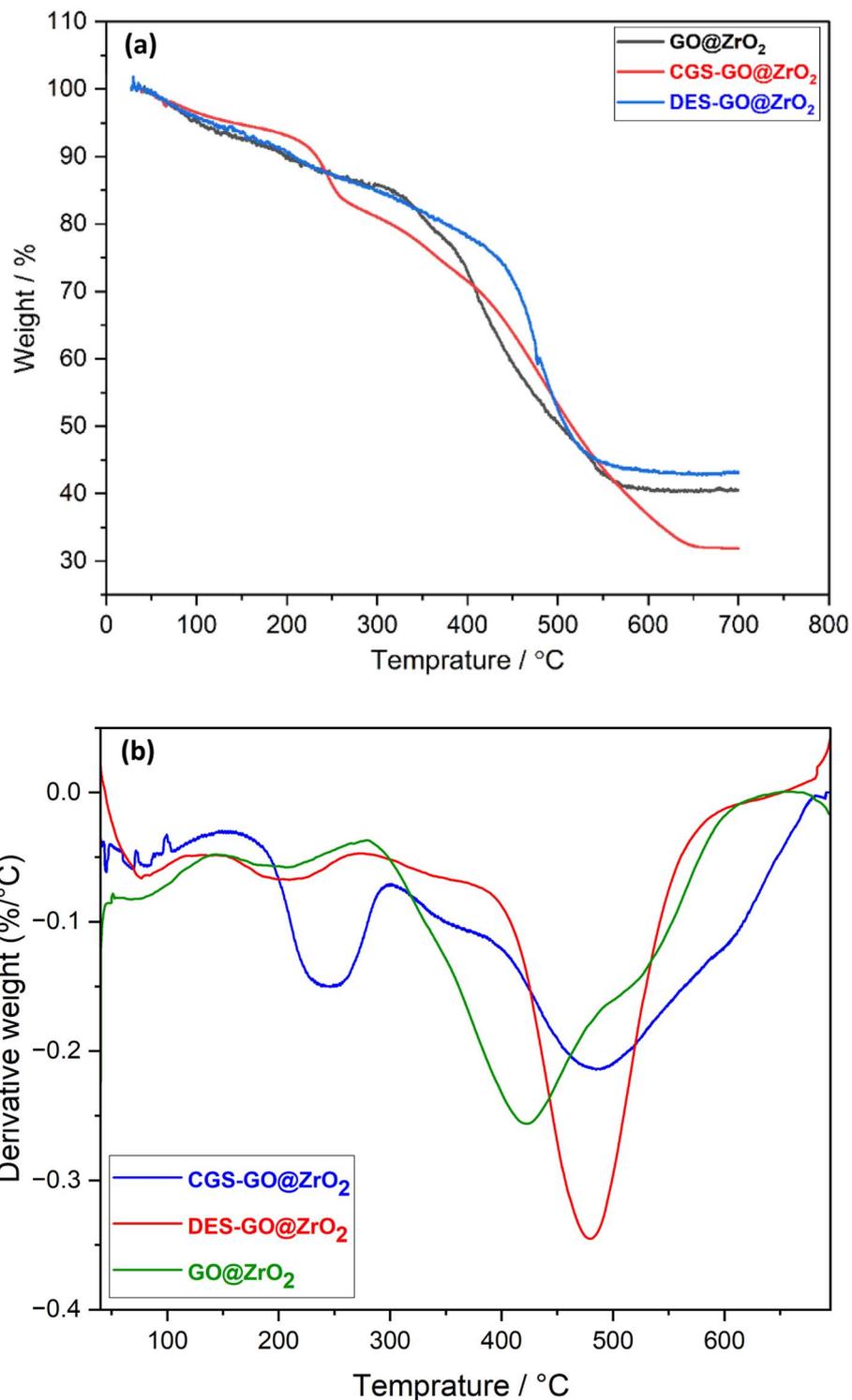
Fig. 5 (a) Thermograms and (b) derivative thermograms of GO@ZrO$_2$ and CGS/DES modified nanocomposites.

values at different time intervals (Q_t) are plotted against time (t) and such profiles are shown in Fig. 10a & b. The data have been used to obtain Q_e (amount of MB adsorbed per gram of the composite after attaining equilibrium). Various kinetic models (*pseudo*-first order, *pseudo*-second order, and intraparticle diffusion model) have been applied to reveal adsorption kinetics. The well-known Lagergren equation is widely used for

liquid and solid systems to deal with pseudo-first order kinetics.[101]

3.5.1 *Pseudo*-first order kinetic model.
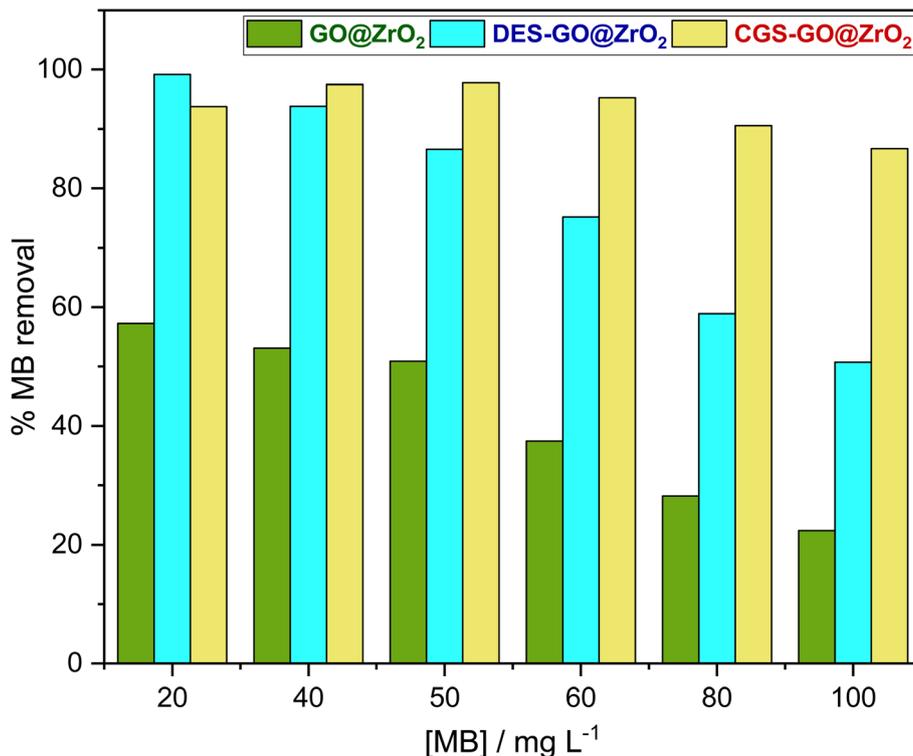
$$\ln(Q_e - Q_t) = \ln Q_e - k_1 t \qquad (4)$$

Fig. 6 Variation of % MB removal from background solution (20 ml, after 60 m) with different initial concentrations of MB (20−100 mg L^{-1}) at 30 ± 0.1 °C: GO@ZrO$_2$ (2 mg ml^{-1}); DES-GO@ZrO$_2$ (2 mg ml^{-1}) and CGS-GO@ZrO$_2$ (10 mg ml^{-1}).

where k_1 (min^{-1}) represents the *pseudo*-first order rate constant for the MB adsorption. Q_e and k_1 can be obtained from the slope and intercept of $\log(Q_e - Q_t)$ *vs.* t plots (Fig. S2a & b†). The computed data related to this model are compiled in Table 1. A perusal of Fig. 10 clearly depicts that kinetic data cannot be fitted in the present model (with both the NCs, Fig. 10a & b, Table 1) and hence other models are also checked. The square of the correlation coefficient (R^2) values, for different initial MB concentrations, are much lower than one and hence denies the appropriateness of the *pseudo*-first order kinetic model. This is also confirmed due to distinct variations in the value of experimentally obtained Q_e and theoretically obtained Q_e (Table 1).

3.5.2   *Pseudo*-second order kinetic model. In the process of finding the correctness of the kinetic model, the data of MB adsorption, with both NCs, were fitted to the *pseudo*-second order kinetic equation,[102]

$$\frac{t}{Q_t} = \frac{1}{k_2 Q_e^2} + \frac{t}{Q_e} \tag{5}$$

where k_2 (g mg^{-1} min^{-1}), the second order rate constant, and Q_e have been computed from a straight-line plot (Fig. S3a & b)† of t/Q_t *vs.* t (using the slope and intercept). When $t \to 0$, the adsorption rate becomes the initial adsorption speed. The data computed for this model are compiled in Table 1. Better R^2 values ($\sim$1) indicate the suitability of the *pseudo*-second order kinetic model to understand the adsorption kinetics of MB on both modified NCs (CGS-GO@ZrO$_2$ and DES-GO@ZrO$_2$).

3.5.3   Intraparticle diffusion kinetic model. Another kinetic model has also been used to interpret adsorption behaviour. This model also considers the diffusion process of the adsorbate in addition to concentration variation. The well-known expression[103] of the present model is as follows,

$$Q_t = k_i t^{1/2} + C_i \tag{6}$$

k_i is the intraparticle velocity constant (mg g^{-1} min$^{1/2}$) and C_i is a constant that is related to boundary layer thickness/ diffusion. Q_t *vs.* $t_{\frac{1}{2}}$ provides a linear plot (Fig. S4a & b)† whose slope and intercept can be used to obtain k_i and C_i. The computed values of k_i, C_i, and R^2 are summarized in Table 1. Looking at the fitted data and R^2 values (far less than 1), one can be observe that pore/surface diffusion is not the only factor but other routes such as film diffusion may also be involved.

From a perusal of all the fitted data in different kinetic models with both the NCs (Table 1), it can be seen that better fitting (Fig. S3†) and acceptable R^2 values are produced with the *pseudo*-second order kinetic model, which hints that this model is probably followed in the present adsorption of MB on both the modified NC surfaces.

3.6   Adsorption isotherm

The applicability of different adsorption isotherm models (at 30 ± 0.1 °C) has been checked by considering Freundlich, Langmuir, and Temkin models.
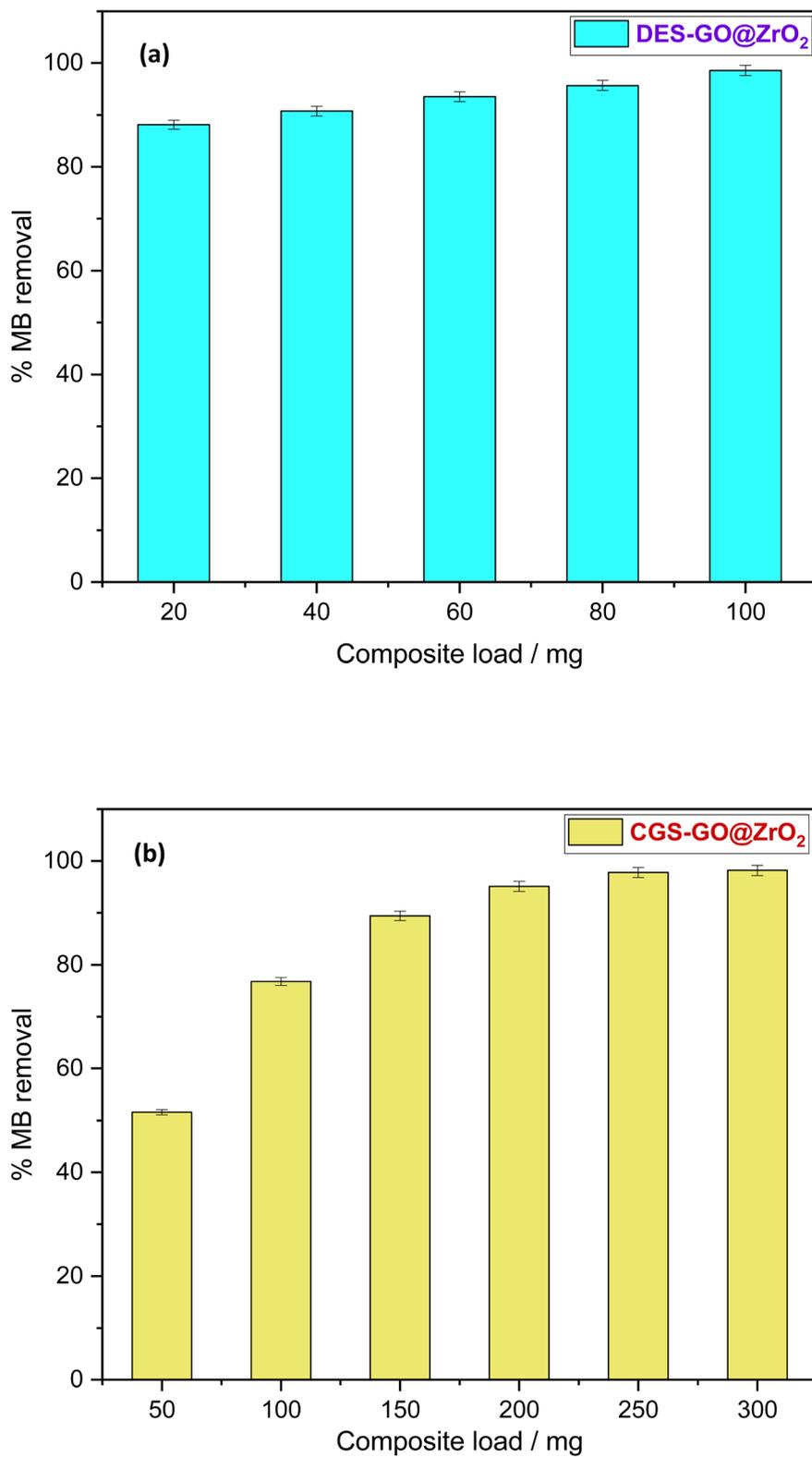
Fig. 7 Optimisation of composite dosages for MB adsorption (20 ml solution, after 60 m): (a) DES-GO@ZrO$_2$ (with 20 mg L^{-1} MB) and (b) CGS-GO@ZrO$_2$ (with 50 mg L^{-1} MB) at 30 ± 0.1 °C.

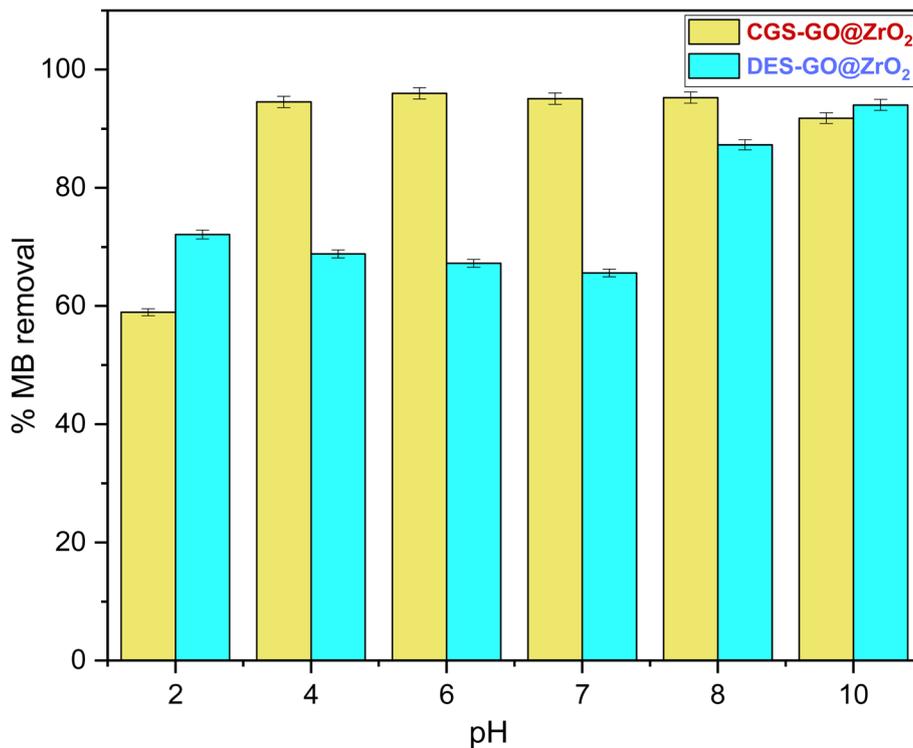**Fig. 8** (a) Influence of pH (2–10) on MB adsorption (20 ml solution, after 60 m) by DES-GO@ZrO$_2$ (2 mg ml^{-1} dosage, with 20 mg L^{-1} MB) and (b) CGS-GO@ZrO$_2$ (10 mg ml^{-1} dosage, with 50 mg L^{-1} MB) at 30 $\pm$ 0.1 °C.
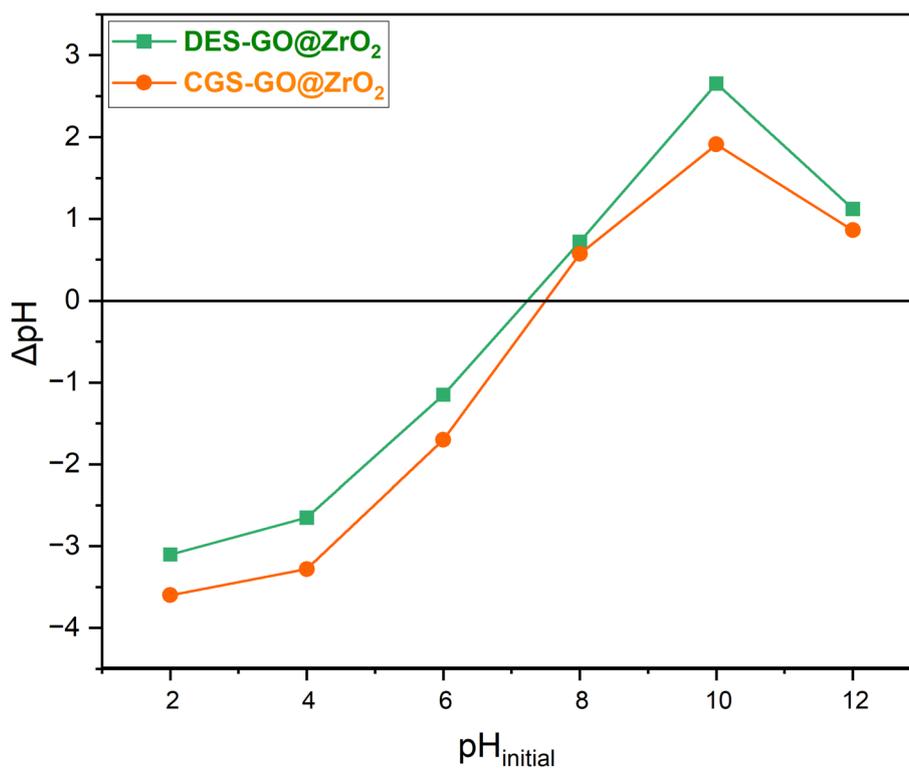
Fig. 9 Variation of ΔpH *vs.* pH$_{initial}$ for DES-GO@ZrO$_2$ (50 mg/20 ml KNO$_3$ solution) and CGS-GO@ZrO$_2$ (50 mg/20 ml KNO$_3$ solution) at 30 $\pm$ 0.1 °C.
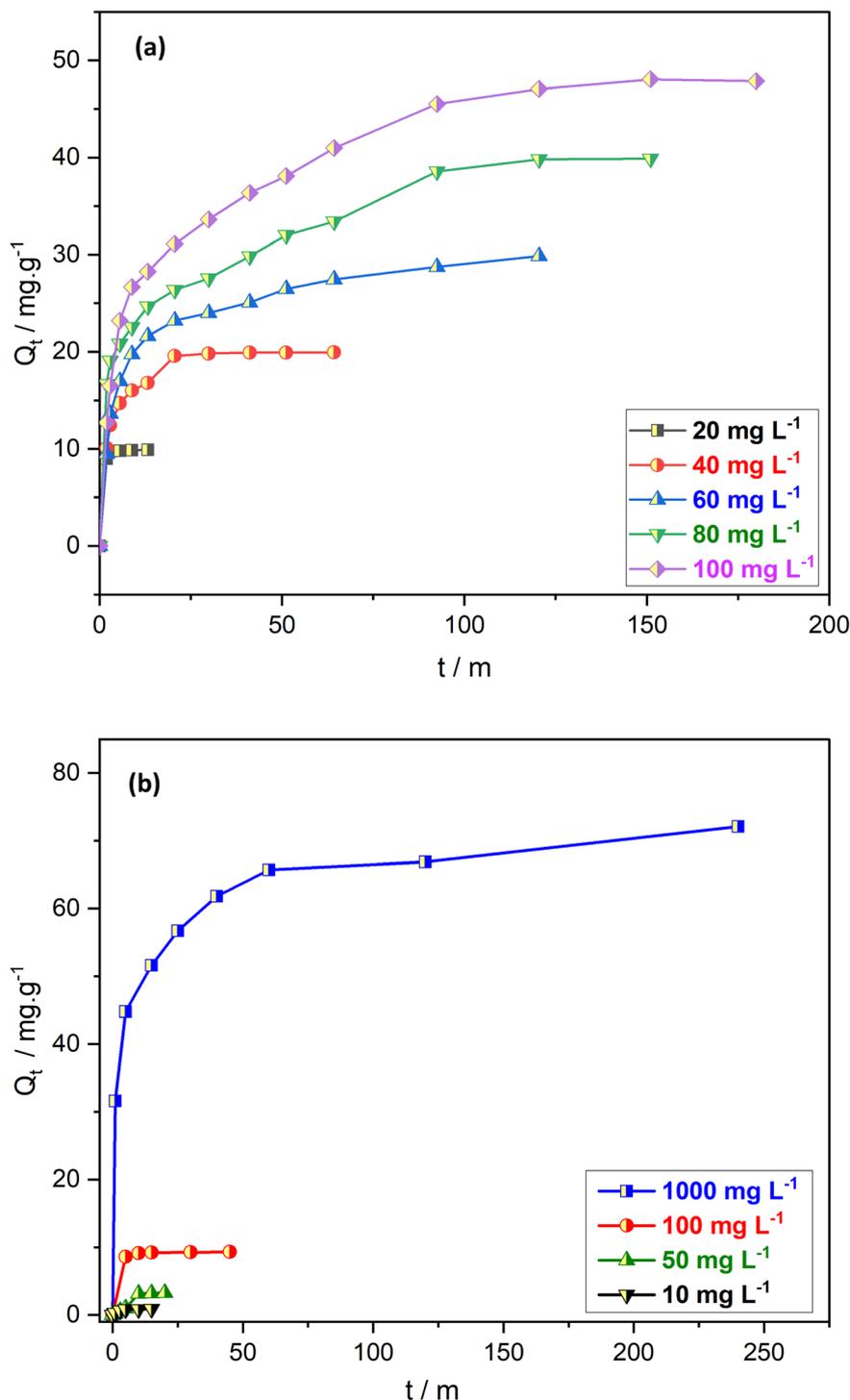
Fig. 10 Variation of adsorption capacity (Q_t) with contact time for various starting MB concentrations (10–1000 mg L^{-1}): (a) DES-GO@ZrO$_2$ (2 mg ml^{-1} dosage, 20 ml solution of MB) and (b) CGS-GO@ZrO$_2$ (10 mg ml^{-1} dosage, 20 ml solution of MB) at 30 ± 0.1 °C.

3.6.1 Freundlich isotherm. According to this adsorption model, the surface of the composite is heterogeneous and assists in multilayer adsorption. Mathematically, the Freundlich isotherm model can be expressed[104] as under,

$$\log Q_e = \log K_{FI} + \frac{1}{n} \log C_e \qquad (7)$$

where K_{FI} (mg g^{-1}) and n are the Freundlich adsorption constant and adsorption potency, respectively. n decides the spontaneity and reversibility of the process ($0 < 1/n < 1$, spontaneous; $1/n > 1$, non-spontaneous; $1/n = 1$, non-reversible). K_{FI} and n can be computed from the intercept and slope of the plots of $\log Q_e$ vs. $\log C_e$ (Fig. S5†) where C_e is the equilibrium [MB]. The related data are summarized in

Table 2 Fitted adsorption data of MB on DES-GO@ZrO$_2$ and CGS-GO@ZrO$_2$ using various models

Isotherms	Parameters	DES-GO@ZrO$_2$	CGS-GO@ZrO$_2$
Freundlich	K_{Fl} (mg g^{-1})	14.24	1.51
	n	0.15	0.73
	R^2	0.936	0.885
Langmuir	Q_m (mg g^{-1})	22.94	15.91
	b (L mg^{-1})	4.731	0.127
	R^2	0.971	0.995
	R_{EP}	0.0104–0.0021	0.4405–0.0078
Temkin	K_T (L g^{-1})	359.50	3.50
	2.303 RT/b	2.595	2.251
	R^2	0.979	0.816

Table 2. The poor R^2 values clearly indicate the non-applicability of the Freundlich adsorption model and deny the multilayer adsorption.

3.6.2 Langmuir isotherm. Since the Freundlich adsorption isotherm model fails to fit the present adsorption data of MB, therefore, other models were tested to know the exact mechanism of MB adsorption. Another well-known adsorption model namely, the Langmuir isotherm,[105] has been considered to fit. The Langmuir isotherm is represented by,

$$\frac{1}{Q_e} = \frac{1}{Q_m} \times \frac{1}{b} \times \frac{1}{C_e} + \frac{1}{Q_m} \quad (8)$$

where Q_m is the content of MB to form a uni-layer (mg g^{-1}) and b (L mg^{-1}) is a constant which represents adsorption energy. A plot of $1/Q_e$ vs. $1/C_e$ results in a straight line with a slope (gives 1/b Q_m) and intercept ($1/Q_m$) (Fig. S6†). The values of R^2 were found to be reasonably good and are compiled with other adsorption constants of this model in Table 2. These data indicate the suitability of the Langmuir model for MB adsorption on modified NCs. This was further confirmed by the determination of the equilibrium adsorption parameter (REP)

Table 3 Comparison of removal efficiency of DES-GO@ZrO$_2$ and CGS-GO@ZrO$_2$ with similar materials reported in the literature

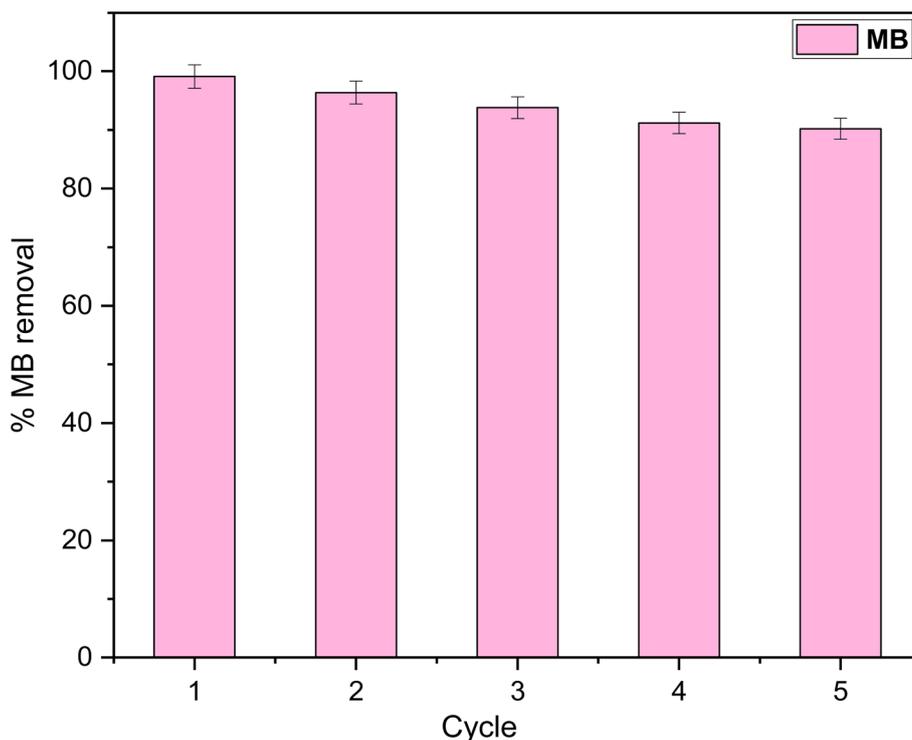| Nanocomposite names	Adsorbent dosage (mg mL^{-1})	Initial MB concentration (ppm)	Adsorption time (min)	Removal efficiency (%)	Ref.
DES-GO@ZrO$_2$	2	20	5	~100%	This work
CGS-GO@ZrO$_2$	10	10	5	82%	This work
Fe$_3$O$_{4-x}$GO	0.28	150	180	97.5%	71
CS/Fe$_3$O$_4$/GO	0.4	5	1200	~25%	109
MGC/GO	1	30	840	96.7%	108
GO/Fe$_3$O$_4$/SiO$_2$	0.25	3.2	10	~65%	110

Fig. 11 Recyclability study of DES-GO@ZrO$_2$ using 50 ml of ethanol for each cycle (up to 5 cycles).
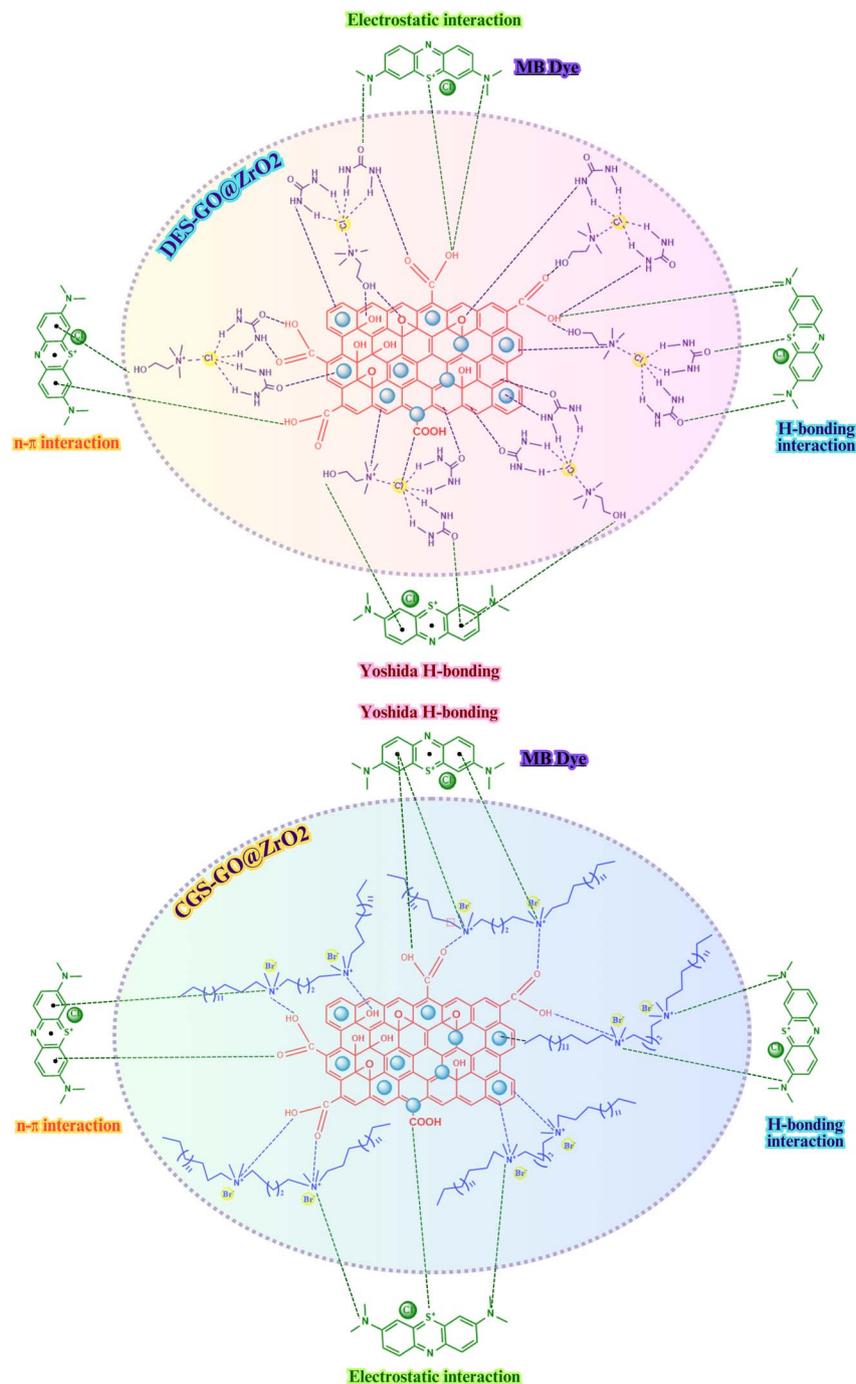
Scheme 2 Depiction of MB adsorption on modified NCs *via* different modes of interactions.

which is related to b and C_i by using the following mathematical expression,

$$R_{EP} = \frac{1}{1 + bC_i} \qquad (9)$$

R_{EP} gives an idea about the favourability of adsorption equilibrium. The ranges of R_{EP} for different initial [MB] are also tabulated in Table 2. R_{EP} varies between 0.01 and 0.0021 (for

DES-GO@ZrO$_2$) and 0.4405–0.0078 (for CGS-GO@ZrO$_2$) which proves that monolayer adsorption is taking place spontaneously. Furthermore, NCs provide nearly homogeneous surfaces.

3.6.3 Temkin isotherm. To ensure the applicability of the Langmuir model, the adsorption data were also fitted into another well-known model, known as the Temkin isotherm.[106] This model asserts that the heat of adsorption lowers linearly during the transfer of the adsorbate toward the adsorbent surface, and the model can be expressed mathematically as,

$$Q_e = 2.303 \frac{RT}{b}(\log K_T + \log C_e) \qquad (10)$$

The term K_T (L g^{-1}) is the Temkin constant related to the energy involved in the binding of MB to modified NC. The value of RT/b gives insight into the nature of the adsorption process. These values were obtained from the slope and intercept of the plot of Q_e vs. log C_e (Fig. S7†). If $RT/b > 0$, the process can be said to be exothermic and vice versa, while when $RT/b < 0$, means that heat is absorbed during adsorption, i.e., an endothermic process. The values of RT/b, KT, and R^2 are also included in Table 2.

A perusal of isotherm parameters (Table 2) of different adsorption models (mentioned above) indicates that both Langmuir (monolayer adsorption) and Temkin (exothermic) models are equally followed by the MB adsorption data obtained with CGS-GO@ZrO$_2$ and DES-GO@ZrO$_2$ as adsorbents. This indicates that monolayer adsorption of MB is taking place together with heat release. Therefore, the binding strength of MB to DES-GO@ZrO$_2$ seems higher than to CGS-GO@ZrO$_2$.

3.7 Comparison of MB adsorption with similar composite materials

Table 3 shows the compilation of the adsorption/removal data of MB with similar composites.[107–110] Among two modified composites (for faster removal), DES-GO@ZrO$_2$ has been found to be superior to CGS-GO@ZrO$_2$. A perusal of comparative data shows that DES-GO@ZrO$_2$ shows good adsorption efficiency (close to 100%) within a short time (5 m) though the DES-GO@ZrO$_2$ dose was slightly towards the higher side. However, the adsorption time column in Table 3 clearly shows that the DES-GO@ZrO$_2$ can be a preferred candidate for the faster removal of MB or similar materials (yet to be checked). Based on this observation, DES-GO@ZrO$_2$ has been chosen for the recyclability study.

3.8 Recyclability/reusability study

For an adsorbent, the potential is not only determined by its adsorption/removal efficiency but also by reusability (to control the economy of the process) one after another cycle.[111-113] Here, MB adsorbed DES-GO@ZrO$_2$ has been recycled by washing it with various solvents (water, 0.1 M HCl, 0.1 M NaOH, methanol, and ethanol). The washing ability of adsorbed MB is shown in Fig. S8.† Ethanol has been found to be a better solvent to desorb MB from the said composite ($R_e \sim 86\%$). Fig. 11 shows the adsorption–desorption efficiency of the MB adsorbed DES-GO@ZrO$_2$. It can be noticed that the composite can be efficiently recycled/reused for at least 5 successive cycles with ethanol as the recharging solvent. The efficiency of the process corroborates the physical interaction involved in the adsorption process of MB. Better adsorption capabilities even after 5 cycles suggest that DES-GO@ZrO$_2$ can perform as a potential adsorbent for MB or MB derivatives.[114]

3.9 Mechanism of MB adsorption

Preliminary TEM data (Fig. 3) show that ZrO$_2$ sits on the surface of GO sheets with a homogenous distribution. CGS and DES contain certain groups which can interact with the GO@ZrO$_2$ composite via electrostatic and hydrophobic interactions. MB will be adsorbed on the modified surface of the composite via various interactions represented in Scheme 2. Various active groups are available on the modified NCs which perform an important role in the MB adsorption process. The nature of the NCs is shifted towards hydrophobic (due to hydrocarbon chains available on CGS or DES) which consequently contributes to attracting MB molecules towards the adsorbent surface.

4 Conclusion

DES-GO@ZrO$_2$ has been found to be distinctly better than CGS-GO@ZrO$_2$ for adsorption/removal from an aqueous solution of MB. The adsorption process has been found to be driven by electrostatic/hydrophobic interactions of MB with NC surfaces. The results of the adsorption process follow the Langmuir adsorption isotherm model indicating the homogeneity of the NC surfaces. DES-GO@ZrO$_2$ shows complete adsorption (within 5 m) for MB when compared with other similar adsorbents (Table 3). Kinetic study showed that adsorption-time data follow pseudo-second order kinetics. The recyclability experiment showed that DES-GO@ZrO$_2$ performs well even after the 5th cycle. Ethanol has been found to be a good recharging solvent for the said composite. Furthermore, the information can be used to produce potential commercial filters involving DES-GO@ZrO$_2$ for the faster/effective removal of coloured dyes or colouring material before discarding into running streams (control of water pollution to make it potable for humans, aquatic habitats together with irrigation). The spectrum of application can be enlarged by performing similar studies with other industrial effluents, e.g., paint, textile, leather, or paper.

Abbreviations

DES	Deep eutectic solvent
GO	Graphene oxide
MB	Methylene blue
CGS	Cationic gemini surfactant
NC	Nanocomposite

Conflicts of interest

There is no conflict of interest.

Acknowledgements

References

1 R. K. Joshi, S. Alwarappan, M. Yoshimura, V. Sahajwalla and Y. Nishina, Graphene oxide: the new membrane material, *Appl. Mater. Today*, 2015, **1**, 1–12.

2 S. Maniappan, C. Dutta, D. M. Solís, J. M. Taboada and J. Kumar, Surfactant Directed Synthesis of Intrinsically Chiral Plasmonic Nanostructures and Precise Tuning of Their Optical Activity through Controlled Self-Assembly, *Angew. Chem., Int. Ed.*, 2023, **62**(21), e202300461.

3 N. Baig, I. Kammakakam and W. Falath, Nanomaterials: a review of synthesis methods, properties, recent progress, and challenges, *Adv. Mater.*, 2021, **2**, 1821–1871.

4 A. Ambrosi, C. K. Chua, N. M. Latiff, A. H. Loo, C. H. A. Wong, A. Y. S. Eng, A. Bonanni and M. Pumera, Graphene and its electrochemistry – an update, *Chem. Soc. Rev.*, 2016, **45**, 2458–2493.

5 M. Francisco, A. van den Bruinhorst and M. C. Kroon, Low-Transition-Temperature Mixtures (LTTMs): A New Generation of Designer Solvents, *Angew. Chem., Int. Ed.*, 2013, **52**, 3074–3085.

6 A. Paiva, R. Craveiro, I. Aroso, M. Martins, R. L. Reis and A. R. C. Duarte, Natural Deep Eutectic Solvents – Solvents for the 21st Century, *ACS Sustain. Chem. Eng.*, 2014, **2**, 1063–1071.

7 X. Li, Y.-L. Wang, J. Wen, L. Zheng, C. Qian, Z. Cheng, H. Zuo, M. Yu, J. Yuan, R. Li, W. Zhang and Y. Liao, Porous organic polycarbene nanotrap for efficient and selective gold stripping from electronic waste, *Nat. Commun.*, 2023, **14**, 263.

8 R. Zana and Y. Talmon, Dependence of aggregate morphology on structure of dimeric surfactants, *Nature*, 1993, **362**, 228–230.

9 R. von Ballmoos and W. M. Meier, Zoned aluminium distribution in synthetic zeolite ZSM-5, *Nature*, 1981, **289**, 782–783.

10 R. D. Rogers, Reflections on ionic liquids, *Nature*, 2007, **447**, 917–918.

11 B. Boates, A. M. Teweldeberhan and S. A. Bonev, Stability of dense liquid carbon dioxide, *Proc. Natl. Acad. Sci. U. S. A.*, 2012, **109**, 14808–14812.

12 J. Li, H. Zeng, Z. Zeng, Y. Zeng and T. Xie, Promising Graphene-Based Nanomaterials and Their Biomedical Applications and Potential Risks: A Comprehensive Review, *ACS Biomater. Sci. Eng.*, 2021, **7**, 5363–5396.

13 A. Hirsch, The era of carbon allotropes, *Nat. Mater.*, 2010, **9**, 868–871.

14 P. Ramnani, N. M. Saucedo and A. Mulchandani, Carbon nanomaterial-based electrochemical biosensors for label-free sensing of environmental pollutants, *Chemosphere*, 2016, **143**, 85–98.

15 M. S. Mauter and M. Elimelech, Environmental Applications of Carbon-Based Nanomaterials, *Environ. Sci. Technol.*, 2008, **42**, 5843–5859.

16 J.-T. Wang, C. Chen, E. Wang and Y. Kawazoe, A New Carbon Allotrope with Six-Fold Helical Chains in all-sp2 Bonding Networks, *Sci. Rep.*, 2014, **4**, 4339.

17 B. F. Machado and P. Serp, Graphene-based materials for catalysis, *Catal. Sci. Technol.*, 2012, **2**, 54–75.

18 X. Huang, X. Qi, F. Boey and H. Zhang, Graphene-based composites, *Chem. Soc. Rev.*, 2012, **41**, 666–686.

19 L. Jiao, L. Zhang, X. Wang, G. Diankov and H. Dai, Narrow graphene nanoribbons from carbon nanotubes, *Nature*, 2009, **458**, 877–880.

20 O. V. Yazyev and S. G. Louie, Electronic transport in polycrystalline graphene, *Nat. Mater.*, 2010, **9**, 806–809.

21 C. Cheng and D. Li, Solvated Graphenes: An Emerging Class of Functional Soft Materials, *Adv. Mater.*, 2013, **25**, 13–30.

22 I. Chowdhury, M. C. Duch, N. D. Mansukhani, M. C. Hersam and D. Bouchard, Colloidal Properties and Stability of Graphene Oxide Nanomaterials in the Aquatic Environment, *Environ. Sci. Technol.*, 2013, **47**, 6288–6296.

23 F. Mouhat, F.-X. Coudert and M.-L. Bocquet, Structure and chemistry of graphene oxide in liquid water from first principles, *Nat. Commun.*, 2020, **11**, 1566.

24 J. D. Buron, F. Pizzocchero, P. U. Jepsen, D. H. Petersen, J. M. Caridad, B. S. Jessen, T. J. Booth and P. Bøggild, Graphene mobility mapping, *Sci. Rep.*, 2015, **5**, 12305.

25 Q. Zhou, J. Huang, J. Wang, Z. Yang, S. Liu, Z. Wang and S. Yang, Preparation of a reduced graphene oxide/zirconia nanocomposite and its application as a novel lubricant oil additive, *RSC Adv.*, 2015, **5**, 91802–91812.

26 N. Nasseh, F. S. Arghavan, N. Daglioglu and A. Asadi, Fabrication of novel magnetic CuS/Fe3O4/GO nanocomposite for organic pollutant degradation under visible light irradiation, *Environ. Sci. Pollut. Res.*, 2021, **28**, 19222–19233.

27 N. El-Shafai, M. E. El-Khouly, M. El-Kemary, M. Ramadan, I. Eldesoukey and M. Masoud, Graphene oxide decorated with zinc oxide nanoflower, silver and titanium dioxide nanoparticles: fabrication, characterization, DNA interaction, and antibacterial activity, *RSC Adv.*, 2019, **9**, 3704–3714.

28 K. Thangavelu, C. Aubry and L. Zou, Amphiphilic Janus 3D MoS$_2$/rGO Nanocomposite for Removing Oil from Wastewater, *Ind. Eng. Chem. Res.*, 2021, **60**, 1266–1273.

29 K. Sanjeev Kumar, K. Giribabu, R. Suresh, R. Manigandan, S. Praveen Kumar and V. Narayanan, Bismuth sulphide/reduced graphene oxide nanocomposites as an electrochemical sensing platform for hexanitrodiphenylamine, *Mater. Lett.*, 2021, **283**, 128804.

30 X. Kang, X. Zhu, J. Liu, X. Shu, Y. Huang and J. Qian, Dissolution and precipitation behaviours of graphene

oxide/tricalcium silicate composites, *Composites, Part B*, 2020, **186**, 107800.

31 N. Devi, R. Kumar, S. Singh and R. K. Singh, Recent development of graphene-based composite for multifunctional applications: energy, environmental and biomedical sciences, *Crit. Rev. Solid State Mater. Sci.*, 2022, 1–69.

32 Q. Li, Z. Zhan, S. Jin and B. Tan, Wettable magnetic hypercrosslinked microporous nanoparticle as an efficient adsorbent for water treatment, *Chem. Eng. J.*, 2017, **326**, 109–116.

33 R. S. Das, S. K. Warkhade, A. Kumar, G. S. Gaikwad and A. V. Wankhade, Graphitic carbon nitride @ silver zirconate nanocomposite (gC3N4@Ag2ZrO3): a Type-II heterojunction for an effective visible light photocatalysis and bacterial photo-inactivation, *J. Alloys Compd.*, 2020, **846**, 155770.

34 G. Z. Kyzas, E. A. Deliyanni, D. N. Bikiaris and A. C. Mitropoulos, Graphene composites as dye adsorbents: Review, *Chem. Eng. Res. Des.*, 2018, **129**, 75–88.

35 H. W. Ha, A. Choudhury, T. Kamal, D.-H. Kim and S.-Y. Park, Effect of Chemical Modification of Graphene on Mechanical, Electrical, and Thermal Properties of Polyimide/Graphene Nanocomposites, *ACS Appl. Mater. Interfaces*, 2012, **4**, 4623–4630.

36 Y. Qi, M. Yang, W. Xu, S. He and Y. Men, Natural polysaccharides-modified graphene oxide for adsorption of organic dyes from aqueous solutions, *J. Colloid Interface Sci.*, 2017, **486**, 84–96.

37 Y. Kuang, R. Yang, Z. Zhang, J. Fang, M. Xing and D. Wu, Surfactant-loaded graphene oxide sponge for the simultaneous removal of Cu2+ and bisphenol A from water, *Chemosphere*, 2019, **236**, 124416.

38 W. M. Algothmi, N. M. Bandaru, Y. Yu, J. G. Shapter and A. V. Ellis, Alginate–graphene oxide hybrid gel beads: an efficient copper adsorbent material, *J. Colloid Interface Sci.*, 2013, **397**, 32–38.

39 Z. Wu, H. Zhong, X. Yuan, H. Wang, L. Wang, X. Chen, G. Zeng and Y. Wu, Adsorptive removal of methylene blue by rhamnolipid-functionalized graphene oxide from wastewater, *Water Res.*, 2014, **67**, 330–344.

40 S. Singh, B. Patel, K. Parikh and S. Kumar, Fabrication of Cationic Surfactant (Conventional/Gemini) Functionalized Gr@ZrO₂ Nanocomposite with Faster Adsorbability of an Anionic Azo Dye from Aqueous Solution, *ChemistrySelect*, 2020, **5**, 14230–14238.

41 J. Yuan, A. Luna, W. Neri, C. Zakri, T. Schilling, A. Colin and P. Poulin, Graphene liquid crystal retarded percolation for new high-k materials, *Nat. Commun.*, 2015, **6**, 8700.

42 S. S. Basu, S. Rahut, A. S. Bisht and J. K. Basu, Surfactant-assisted tuning of K2V3O8 nanorods for robust charge dynamics in semiconductor photocatalysis, *Mater. Sci. Semicond. Process.*, 2022, **147**, 106681.

43 V. Agarwal, Y. Fadil, A. Wan, N. Maslekar, B. N. Tran, R. A. Mat Noor, S. Bhattacharyya, J. Biazik, S. Lim and P. B. Zetterlund, Influence of Anionic Surfactants on the Fundamental Properties of Polymer/Reduced Graphene Oxide Nanocomposite Films, *ACS Appl. Mater. Interfaces*, 2021, **13**, 18338–18347.

44 V. Georgakilas, M. Otyepka, A. B. Bourlinos, V. Chandra, N. Kim, K. C. Kemp, P. Hobza, R. Zboril and K. S. Kim, Functionalization of Graphene: Covalent and Non-Covalent Approaches, Derivatives and Applications, *Chem. Rev.*, 2012, **112**, 6156–6214.

45 M. Yusuf, M. A. Khan, M. Otero, E. C. Abdullah, M. Hosomi, A. Terada and S. Riya, Synthesis of CTAB intercalated graphene and its application for the adsorption of AR265 and AO7 dyes from water, *J. Colloid Interface Sci.*, 2017, **493**, 51–61.

46 Y. Wu, H. Luo, H. Wang, C. Wang, J. Zhang and Z. Zhang, Adsorption of hexavalent chromium from aqueous solutions by graphene modified with cetyltrimethylammonium bromide, *J. Colloid Interface Sci.*, 2013, **394**, 183–191.

47 M. Yusuf, M. A. Khan, E. C. Abdullah, M. Elfghi, M. Hosomi, A. Terada, S. Riya and A. Ahmad, Dodecyl sulfate chain anchored mesoporous graphene: synthesis and application to sequester heavy metal ions from aqueous phase, *Chem. Eng. J.*, 2016, **304**, 431–439.

48 X. Wang, M. Li, S. Yang and J. Shan, A novel electrochemical sensor based on TiO2–Ti3C2TX/CTAB/chitosan composite for the detection of nitrite, *Electrochim. Acta*, 2020, **359**, 136938.

49 J. Su, S. He, Z. Zhao, X. Liu and H. Li, Efficient preparation of cetyltrimethylammonium bromide-graphene oxide composite and its adsorption of Congo red from aqueous solutions, *Colloids Surf., A*, 2018, **554**, 227–236.

50 J. Xu, X. Cai and F. Shen, Preparation and property of UV-curable polyurethane acrylate film filled with cationic surfactant treated graphene, *Appl. Surf. Sci.*, 2016, **379**, 433–439.

51 K. Taleb, I. Pillin, Y. Grohens and S. Saidi-Besbes, Gemini surfactant modified clays: effect of surfactant loading and spacer length, *Appl. Clay Sci.*, 2018, **161**, 48–56.

52 S. Kalam, S. A. Abu-Khamsin, M. S. Kamal, S. M. S. Hussain, K. Norrman, M. Mahmoud and S. Patil, Adsorption Mechanisms of a Novel Cationic Gemini Surfactant onto Different Rocks, *Energy Fuels*, 2022, **36**, 5737–5748.

53 H. Wang, R. Li, Q. Wu, G. Fei, Y. Li, M. Zou and L. Sun, Gemini surfactant-assisted fabrication of graphene oxide/polyaniline towards high-performance waterborne anti-corrosive coating, *Appl. Surf. Sci.*, 2021, **565**, 150581.

54 S. He, X. Liu, P. Yan, A. Wang, J. Su and X. Su, Preparation of gemini surfactant/graphene oxide composites and their superior performance for Congo red adsorption, *RSC Adv.*, 2019, **9**, 4908–4916.

55 Y.-Y. Lyu, S. H. Yi, J. K. Shon, S. Chang, L. S. Pu, S.-Y. Lee, J. E. Yie, K. Char, G. D. Stucky and J. M. Kim, Highly Stable Mesoporous Metal Oxides Using Nano-Propping Hybrid Gemini Surfactants, *J. Am. Chem. Soc.*, 2004, **126**, 2310–2311.

56 S. K. Yadav, K. Parikh and S. Kumar, Mixed micelle formation of cationic gemini surfactant with anionic bile

salt: a PAH solubilization study, *Colloids Surf., A*, 2017, **522**, 105–112.

57 K. U. Din, W. Fatma, Z. A. Khan and A. A. Dar, H NMR and Viscometric Studies on Cationic Gemini Surfactants in Presence of Aromatic Acids and Salts, *J. Phys. Chem. B*, 2007, **111**, 8860–8867.

58 S. Singh, A. Bhadoria, K. Parikh, S. K. Yadav, S. Kumar, V. K. Aswal and S. Kumar, Self-Assembly in Aqueous Oppositely Charged Gemini Surfactants: A Correlation between Morphology and Solubilization Efficacy, *J. Phys. Chem. B*, 2017, **121**, 8756–8766.

59 F. M. Menger and J. S. Keiper, *Angew. Chem., Int. Ed.*, 2000, **39**, 1906–1920.

60 S. Kumar and K. Parikh, *Influence of Temperature and Salt on Association and Thermodynamic Parameters of Micellization of a Cationic Gemini Surfactant*, 2012, vol. 1.

61 Md. S. Alam, A. Mohammed Siddiq and M. Ali, The micellization studies of cationic gemini surfactant, hexanediyl-1,6-bis(dimethylcetylammonium bromide solutions by conductometric, tensiometric, dye solubilisation, FTIR and 1H NMR: the influence of adenosine and temperature, *J. Mol. Liq.*, 2022, **349**, 118386.

62 A. Mohammed Siddiq, R. Thangam, B. Madhan and Md. S. Alam, Green (gemini) surfactant mediated gold nanoparticles green synthesis: effect on triple negative breast cancer cells, *Nano-Struct. Nano-Objects*, 2019, **19**, 100373.

63 A. M. Siddiq, R. Thangam, B. Madhan and M. S. Alam, Counterion coupled (COCO) gemini surfactant capped Ag/Au alloy and core–shell nanoparticles for cancer therapy, *RSC Adv.*, 2019, **9**, 37830–37845.

64 M. S. Alam, A. M. Siddiq, D. Natarajan, M. S. Kiran and G. Baskar, Physicochemical properties and bioactivity studies of synthesized counterion coupled (COCO) gemini surfactant, 1,6-bis(N,N-hexadecyldimethylammonium) adipate, *J. Mol. Liq.*, 2019, **273**, 16–26.

65 Md. S. Alam and A. M. Siddiq, Density, dynamic viscosity, and kinematic viscosity studies of aqueous solution of a cationic gemini surfactant, hexanediyl-1,6-bis(dimethylcetylammonium bromide (16-6-16): influence of electrolytes and temperature, *J. Mol. Liq.*, 2017, **242**, 1075–1084.

66 S. Chen, W. Wang and W. Xu, A Photoresponsive azobenzene-graphene-gold nanocomposite using cationic azobenzene-surfactant as stabilizers and its electrochemical behavior, *Mater. Lett.*, 2016, **180**, 196–199.

67 B. B. Hansen, S. Spittle, B. Chen, D. Poe, Y. Zhang, J. M. Klein, A. Horton, L. Adhikari, T. Zelovich, B. W. Doherty, B. Gurkan, E. J. Maginn, A. Ragauskas, M. Dadmun, T. A. Zawodzinski, G. A. Baker, M. E. Tuckerman, R. F. Savinell and J. R. Sangoro, Deep Eutectic Solvents: A Review of Fundamentals and Applications, *Chem. Rev.*, 2021, **121**, 1232–1285.

68 M. Rabiul Islam, F. Warsi, M. Sayem Alam and M. Ali, Solvatochromic behaviour of coumarin 102 in PEGs + ionic liquid/water solutions: Role of solute-solvent or solvent-solvent interactions, *J. Mol. Liq.*, 2021, **334**, 116483.

69 F. Warsi, M. R. Islam, M. S. Alam and M. Ali, Exploring the effect of hydrophobic ionic liquid on aggregation, micropolarity and microviscosity properties of aqueous SDS solutions, *J. Mol. Liq.*, 2020, **310**, 113132.

70 M. R. Islam, S. Shakya, A. Selim, M. S. Alam and M. Ali, Solvatochromic Absorbance and Fluorescence Probe Behavior within Ionic Liquid + γ-Butyrolactone Mixture, *J. Chem. Eng. Data*, 2019, **64**, 4169–4180.

71 N. Mehrabi, U. F. Abdul Haq, M. T. Reza and N. Aich, Application of deep eutectic solvent for conjugation of magnetic nanoparticles onto graphene oxide for lead(II) and methylene blue removal, *J. Environ. Chem. Eng.*, 2020, **8**, 104222.

72 M. Hejazi Khah, P. Jamshidi and F. Shemirani, Applicability of an eco-friendly deep eutectic solvent loaded onto magnetic graphene oxide to preconcentrate trace amount of indigotin blue dye, *J. Mol. Liq.*, 2021, **342**, 117346.

73 R. Bavandpour, M. Rajabi, H. Karimi-Maleh and A. Asghari, Application of deep eutectic solvent and SWCNT-ZrO2 nanocomposite as conductive mediators for the fabrication of simple and rapid electrochemical sensor for determination of trace anti-migration drugs, *Microchem. J.*, 2021, **165**, 106141.

74 C.-W. Lien, B. Vedhanarayanan, J.-H. Chen, J.-Y. Lin, H.-H. Tsai, L.-D. Shao and T.-W. Lin, Optimization of acetonitrile/water content in hybrid deep eutectic solvent for graphene/MoS2 hydrogel-based supercapacitors, *Chem. Eng. J.*, 2021, **405**, 126706.

75 D. A. Pethsangave, R. V. Khose, P. H. Wadekar and S. Some, Deep Eutectic Solvent Functionalized Graphene Composite as an Extremely High Potency Flame Retardant, *ACS Appl. Mater. Interfaces*, 2017, **9**, 35319–35324.

76 N. Mehrabi, H. Lin and N. Aich, Deep eutectic solvent functionalized graphene oxide nanofiltration membranes with superior water permeance and dye desalination performance, *Chem. Eng. J.*, 2021, **412**, 128577.

77 T. Cun, C. Dong and Q. Huang, Ionothermal precipitation of highly dispersive ZnO nanoparticles with improved photocatalytic performance, *Appl. Surf. Sci.*, 2016, **384**, 73–82.

78 M. Hayyan, A. Abo-Hamad, M. A. AlSaadi and M. A. Hashim, Functionalization of graphene using deep eutectic solvents, *Nanoscale Res. Lett.*, 2015, **10**, 324.

79 Y. Huang, Y. Wang, Q. Pan, Y. Wang, X. Ding, K. Xu, N. Li and Q. Wen, Magnetic graphene oxide modified with choline chloride-based deep eutectic solvent for the solid-phase extraction of protein, *Anal. Chim. Acta*, 2015, **877**, 90–99.

80 M. A. Shannon, P. W. Bohn, M. Elimelech, J. G. Georgiadis, B. J. Mariñas and A. M. Mayes, Science and technology for water purification in the coming decades, *Nature*, 2008, **452**, 301–310.

81 C. Tortajada and P. van Rensburg, Drink more recycled wastewater, *Nature*, 2020, **577**, 26–28.

82 B. Van der Bruggen, Sustainable implementation of innovative technologies for water purification, *Nat. Rev. Chem*, 2021, **5**, 217–218.

83 D. Hoornweg, P. Bhada-Tata and C. Kennedy, Environment: waste production must peak this century, *Nature*, 2013, **502**, 615–617.

84 W. J. Cosgrove and D. P. Loucks, Water management: Current and future challenges and research directions, *Water Resour. Res.*, 2015, **51**, 4823–4839.

85 X.-Z. Tang, Z. Cao, H.-B. Zhang, J. Liu and Z.-Z. Yu, Growth of silver nanocrystals on graphene by simultaneous reduction of graphene oxide and silver ions with a rapid and efficient one-step approach, *Chem. Commun.*, 2011, **47**, 3084.

86 A. Ahmad, S. N. A. M. Jamil, T. S. Y. Choong, A. H. Abdullah, N. H. Faujan, A. A. Adeyi, R. Daik and N. Othman, Removal of Cationic Dyes by Iron Modified Silica/Polyurethane Composite: Kinetic, Isotherm and Thermodynamic Analyses, and Regeneration via Advanced Oxidation Process, *Polymers*, 2022, **14**, 5416.

87 A. P. Nambiar, R. Pillai, Y. Vadikkeettil, M. Sanyal and P. S. Shrivastav, Glutaraldehyde-crosslinked poly(vinyl alcohol)/halloysite composite films as adsorbent for methylene blue in water, *Mater. Chem. Phys.*, 2022, **291**, 126752.

88 A. H. Jawad, A. S. Abdulhameed, L. D. Wilson, M. A. K. M. Hanafiah, W. I. Nawawi, Z. A. ALOthman and M. Rizwan Khan, Fabrication of Schiff's Base Chitosan-Glutaraldehyde/Activated Charcoal Composite for Cationic Dye Removal: Optimization Using Response Surface Methodology, *J. Polym. Environ.*, 2021, **29**, 2855–2868.

89 J. Iqbal, N. S. Shah, M. Sayed, N. K. Niazi, M. Imran, J. A. Khan, Z. U. H. Khan, A. G. S. Hussien, K. Polychronopoulou and F. Howari, Nano-zerovalent manganese/biochar composite for the adsorptive and oxidative removal of Congo-red dye from aqueous solutions, *J. Hazard. Mater.*, 2021, **403**, 123854.

90 S. R. Lakhotia, M. Mukhopadhyay and P. Kumari, Cerium oxide nanoparticles embedded thin-film nanocomposite nanofiltration membrane for water treatment, *Sci. Rep.*, 2018, **8**, 4976.

91 E. L. Smith, A. P. Abbott and K. S. Ryder, Deep Eutectic Solvents (DESs) and Their Applications, *Chem. Rev.*, 2014, **114**, 11060–11082.

92 D. Hirpara, B. Patel, V. Chavda, A. Desai and S. Kumar, Micellization and clouding behaviour of an ionic surfactant in a deep eutectic solvent: a case of the reline-water mixture, *J. Mol. Liq.*, 2022, **364**, 119991.

93 D. C. Marcano, D. V. Kosynkin, J. M. Berlin, A. Sinitskii, Z. Sun, A. Slesarev, L. B. Alemany, W. Lu and J. M. Tour, Improved Synthesis of Graphene Oxide, *ACS Nano*, 2010, **4**, 4806–4814.

94 W. S. Hummers and R. E. Offeman, Preparation of Graphitic Oxide, *J. Am. Chem. Soc.*, 1958, **80**, 1339.

95 S. S. Tripathy and S. B. Kanungo, Adsorption of Co2+, Ni2+, Cu2+ and Zn2+ from 0.5 M NaCl and major ion sea water on a mixture of δ-MnO2 and amorphous FeOOH, *J. Colloid Interface Sci.*, 2005, **284**, 30–38.

96 J. Liu, X. Meng, Y. Hu, D. Geng, M. N. Banis, M. Cai, R. Li and X. Sun, Controlled synthesis of Zirconium Oxide on graphene nanosheets by atomic layer deposition and its growth mechanism, *Carbon*, 2013, **52**, 74–82.

97 X. Luo, C. Wang, L. Wang, F. Deng, S. Luo, X. Tu and C. Au, Nanocomposites of graphene oxide-hydrated zirconium oxide for simultaneous removal of As(III) and As(V) from water, *Chem. Eng. J.*, 2013, **220**, 98–106.

98 R. A. K. Rao, S. Singh, B. R. Singh, W. Khan and A. H. Naqvi, Synthesis and characterization of surface modified graphene–zirconium oxide nanocomposite and its possible use for the removal of chlorophenol from aqueous solution, *J. Environ. Chem. Eng.*, 2014, **2**, 199–210.

99 T. Aissaoui, Novel Contribution to the Chemical Structure of Choline Chloride Based Deep Eutectic Solvents, *Pharm. Anal. Acta*, 2015, **6**(11), 1000448.

100 J. T. Adeleke, T. Theivasanthi, M. Thiruppathi, M. Swaminathan, T. Akomolafe and A. B. Alabi, Photocatalytic degradation of methylene blue by ZnO/NiFe2O4 nanoparticles, *Appl. Surf. Sci.*, 2018, **455**, 195–200.

101 H. Yuh-Shan, Citation review of Lagergren kinetic rate equation on adsorption reactions, *Scientometrics*, 2004, **59**, 171–177.

102 A. E. Ofomaja, E. B. Naidoo and S. J. Modise, Dynamic studies and pseudo-second order modeling of copper(II) biosorption onto pine cone powder, *Desalination*, 2010, **251**, 112–122.

103 V. Selen, Ö. Güler, D. Özer and E. Evin, Synthesized multi-walled carbon nanotubes as a potential adsorbent for the removal of methylene blue dye: kinetics, isotherms, and thermodynamics, *Desalin. Water Treat.*, 2016, **57**, 8826–8838.

104 D. Robati, B. Mirza, M. Rajabi, O. Moradi, I. Tyagi, S. Agarwal and V. K. Gupta, Removal of hazardous dyes-BR 12 and methyl orange using graphene oxide as an adsorbent from aqueous phase, *Chem. Eng. J.*, 2016, **284**, 687–697.

105 Y. Liu, Some consideration on the Langmuir isotherm equation, *Colloids Surf., A*, 2006, **274**, 34–36.

106 M. Saxena, N. Sharma and R. Saxena, Highly efficient and rapid removal of a toxic dye: adsorption kinetics, isotherm, and mechanism studies on functionalized multiwalled carbon nanotubes, *Surf. Interfaces*, 2020, **21**, 100639.

107 L. Cui, X. Guo, Q. Wei, Y. Wang, L. Gao, L. Yan, T. Yan and B. Du, Removal of mercury and methylene blue from aqueous solution by xanthate functionalized magnetic graphene oxide: sorption kinetic and uptake mechanism, *J. Colloid Interface Sci.*, 2015, **439**, 112–120.

108 H. Shi, W. Li, L. Zhong and C. Xu, Methylene Blue Adsorption from Aqueous Solution by Magnetic Cellulose/Graphene Oxide Composite: Equilibrium, Kinetics, and Thermodynamics, *Ind. Eng. Chem. Res.*, 2014, **53**, 1108–1118.

109 H. V Tran, L. T. Bui, T. T. Dinh, D. H. Le, C. D. Huynh and A. X. Trinh, Graphene oxide/Fe3O4/chitosan nanocomposite: a recoverable and recyclable adsorbent for organic dyes removal. Application to methylene blue, *Mater. Res. Express*, 2017, **4**, 035701.

110 S. Yang, T. Zeng, Y. Li, J. Liu, Q. Chen, J. Zhou, Y. Ye and B. Tang, Preparation of Graphene Oxide Decorated Fe_3O_4@SiO_2 Nanocomposites with Superior Adsorption Capacity and SERS Detection for Organic Dyes, *J. Nanomater.*, 2015, **2015**, 1–8.

111 C. Liu, A. M. Omer and X. Ouyang, Adsorptive removal of cationic methylene blue dye using carboxymethyl cellulose/k-carrageenan/activated montmorillonite composite beads: isotherm and kinetic studies, *Int. J. Biol. Macromol.*, 2018, **106**, 823–833.

112 G. R. Mahdavinia, M. Soleymani, M. Sabzi, H. Azimi and Z. Atlasi, Novel magnetic polyvinyl alcohol/laponite RD nanocomposite hydrogels for efficient removal of methylene blue, *J. Environ. Chem. Eng.*, 2017, **5**, 2617–2630.

113 L. M. Sanchez, R. P. Ollier and V. A. Alvarez, Sorption behavior of polyvinyl alcohol/bentonite hydrogels for dyes removal, *J. Polym. Res.*, 2019, **26**, 142.

114 M. Wainwright, Methylene blue derivatives—suitable photoantimicrobials for blood product disinfection?, *Int. J. Antimicrob. Agents*, 2000, **16**, 381–394.